Low-dose performance of wafer-scale CMOS-based X-ray detectors

Willem H. Maes, Inge M. Peters, Chiel Smit, Yves Kessener, Jan Bosiers
Teledyne DALSA Professional Imaging, High Tech Campus 27, 5656AE Eindhoven, The Netherlands

ABSTRACT

Compared to published amorphous-silicon (TFT) based X-ray detectors, crystalline silicon CMOS-based active-pixel detectors exploit the benefits of low noise, high speed, on-chip integration and featuring offered by CMOS technology. This presentation focuses on the specific advantage of high image quality at very low dose levels.
The measurement of very low dose performance parameters like Detective Quantum Efficiency (DQE) and Noise Equivalent Dose (NED) is a challenge by itself. Second-order effects like defect pixel behavior, temporal and quantization noise effects, dose measurement accuracy and limitation of the x-ray source settings will influence the measurements at very low dose conditions. Using an analytical model to predict the low dose behavior of a detector from parameters extracted from shot-noise limited dose levels is presented. These models can also provide input for a simulation environment for optimizing the performance of future detectors.
In this paper, models for predicting NED and the DQE at very low dose are compared to measurements on different CMOS detectors. Their validity for different sensor and optical stack combinations as well as for different x-ray beam conditions was validated.

Keywords: CMOS imager, X-ray detector, DQE, Noise Equivalent Dose, low dose, modeling

1. INTRODUCTION

CMOS X-ray detectors are composed of wafer-scale image sensors and an optical stack to convert X-ray photons to visible light photons detectable by the sensor. Large area panels are constructed by butting together different sensors with high precision. The CMOS wafers are processed in a standard CMOS imaging process. CMOS sensors are known for their extremely low readout noise performance as well as their flexibility to tune the charge capacity of the pixel. The low readout noise impacts performance parameters like DQE and NED. The readout noise of the sensor together with the conversion gain of optical stack and sensor allows to predict the DQE decrease towards very low dose conditions and also determines the NED of the detector.
In this paper, an analytical model for predicting the DQE at very low dose is derived from parameter measurements performed at shot-noise limited dose levels. Also a new model for calculating the NED is presented. The models are verified with measurements performed on images at different dose levels for four different detector configurations. Two sensor designs with different pixel pitch and three different optical stack configurations were evaluated. The sensors can be operated at two different charge capacity settings, resulting in two different saturation dose levels and readout noise values. In total, eight different combination of readout noise and stack conversion gain values are measured and validated with the models.

2. DESCRIPTION OF THE MODELS

2.1 Noise Equivalent Dose model derivation

The noise equivalent dose (NED) of a detector is defined as the dose at which the quantum noise equals the readout noise; i.e. when the total noise equals √2 times the readout noise. The readout noise in X-ray photons units (*Ne*) can easily be expressed as:

$$Ne = \frac{En}{Cf} \tag{1}$$

Medical Imaging 2015: Physics of Medical Imaging, edited by Christoph Hoeschen, Despina Kontos,
Proc. of SPIE Vol. 9412, 94120C · © 2015 SPIE · CCC code: 1605-7422/15/$18 · doi: 10.1117/12.2081996

with *En* being the readout noise of the sensor in digital numbers (DN) or electrons (e^-) and *Cf* the conversion factor also expressed in DN/X-ray or e^-/X-ray. *Ne* defines the number of X-ray photons needed to enter the pixel to generate a signal equal to the intrinsic detector readout noise. The following expression for NED can be derived using the photon fluence for the X-ray beam:

$$NED = 2*(Ne)^2 * \left(\left\langle \frac{MTF_x^2(f)}{DQE_x(f)_{high\_dose}} \right\rangle + \left\langle \frac{MTF_y^2(f)}{DQE_y(f)_{high\_dose}} \right\rangle \right)^{-1} * \left(\frac{1}{Photon\_fluence * area\_pixel} \right) \quad (2)$$

with $\langle MTF^2(f)/DQE(f)_{high\_dose} \rangle$ representing the average of the normalized noise power spectrum of the detector in the shot noise regime.

Assuming identical noise power components in x and y direction, equation (2) reduces to:

$$NED = 4*(Ne)^2 * \left\langle \frac{MTF^2(f)}{DQE(f)_{high\_dose}} \right\rangle^{-1} * \left(\frac{1}{Photon\_fluence * area\_pixel} \right) \quad (3)$$

Since *En* depends on the sensor design, and the parameters $\langle MTF^2(f)/DQE(f)_{high\_dose} \rangle$ and *Cf* depend on both the optical stack and the sensor properties, this expression can be used to optimize the detector for minimizing NED.

2.2 Modeling DQE for very low dose performance.

At very low dose levels, DQE(f) will drop because the readout noise cannot be neglected any more compared to the quantum noise in the Noise Power Spectrum. This drop in DQE can be modeled separately, knowing the DQE at high dose levels, using the following equation [4]:

$$DQE(f, low\_dose) = R(f, low\_dose) * DQE(f, high\_dose) \quad (4)$$

with *DQE(f,high_dose)* being the DQE value at high dose. *R(f,low_dose)* can easily be expressed as:

$$R(f, low\_dose) = \left[1 + (Ne)^2 * \left(\frac{1}{Dose * Photon\_fluence * area\_pixel} \right) * \left(\frac{DQE(f, high\_dose)}{MTF^2(f)} \right) \right]^{-1} \quad (5)$$

This equation allows to predict the DQE(f) behavior at very low dose from parameters measured at shot-noise limited dose levels. As expected, the parameter *Ne* contributes significantly at very low dose.

2.3 Schematic architecture of the sensor

The detectors are assembled using an array of 8-inch wafer-scale CMOS-based sensors. This enables building single-tile detectors as well as large-area detectors by butting multiple tiles together. In general, the sensor consists of a 2D pixel array with a one-sided readout circuit as shown in Figure 1.

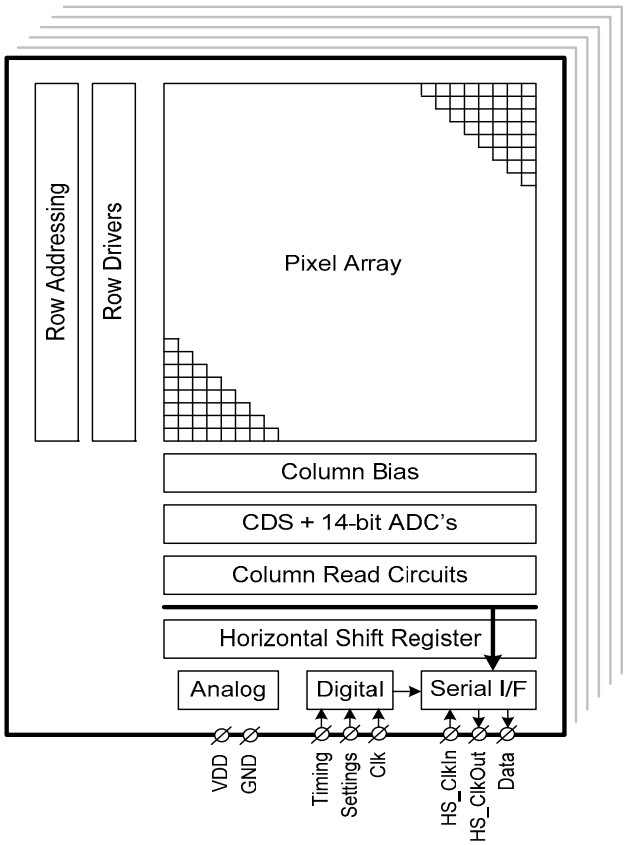

Figure 1: Architecture of the CMOS wafers-size sensor

The readout circuit contains column-parallel ADC circuits, allowing very fast readout speeds of the pixel array. The pixels used for presentation are conventional 3T CMOS pixels allowing the global (i.e. identical for the whole array) selection of multiple charge capacities (full wells) for corresponding saturation dose level selection. A typical pixel architecture with a dual charge capacity feature is shown in Figure **2**, together with its output response characteristics versus input dose .

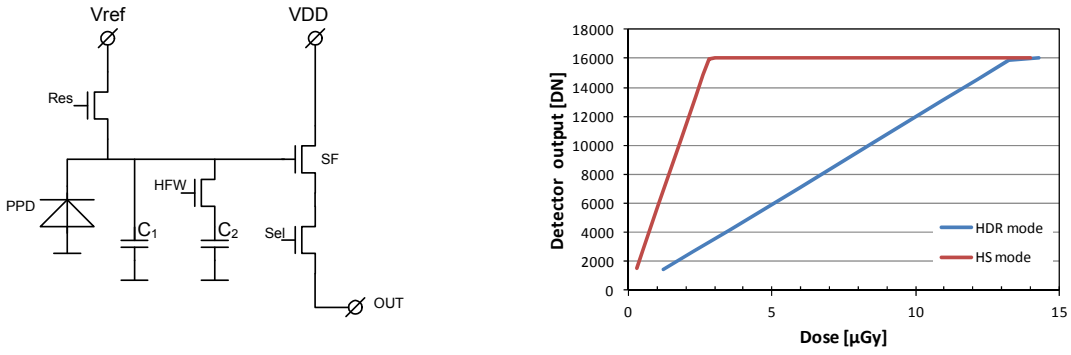

Figure 2: Typical pixel architecture with dual charge capacity and its response in HDR and HS mode.

Selectable charge capacities in the pixel allow to use the same detector for different applications: a small charge capacity delivering the highest signal per X-ray photon for high sensitivity/low dose (HS) applications, and the large charge capacity for high dynamic range/higher dose (HDR) applications. The charge capacity selection is activated by putting the HFW signal in the schematic active, adding an additional capacitance (*C2*) to the pixel charge capacity. The

maximum charge capacity of the pixel and corresponding saturation dose is determined by the designed capacitor at the photo diode node and its voltage swing, which is typically ~2 volt in a 3.3 volt CMOS process. The implementation of this feature does not compromise any other performance parameters of the pixel or imaging array. The on-chip 14-bit analog-to-digital conversion contributes to minimizing the readout noise, and this higher level of system integration is also beneficial for overall system cost and power consumption. In a typical implementation, a readout speed of 30fps is achieved, corresponding to a data rate bandwidth of 72Mpixels/s for a single CMOS sensor.

3. ANALYSIS OF DETECTOR A AND B

3.1 Description of both detectors A and B

Both detectors A and B use a single 15.3 x 15.3 cm^2 wafer-sized CMOS sensor with a 1548*1548 pixel matrix. The pixel size is 99x99μm^2. The design incorporates a dual charge capacity to support different saturation dose levels. The optical stack of both detectors is different: detector A has a Fiber Optic Plate (FOP) glued onto the sensor and a CsI scintillator pressed onto the FOP. Detector B contains the same FOP but the FOP was coated with a CsI scintillator. Comparing both detectors allows investigating DQE and NED performance for different combinations of sensor noise (HS and HDR) and different conversion gains for the optical stack. To determine the factor *Ne* (equation (1)), the following values were extracted from the measurement and summarized in the following table:

Detector		***HS***	***HDR***
A	Readout noise (e-)	145	367
	Conversion gain (e-/X-ray)	490	490
B	Readout noise (e-)	123	340
	Conversion gain (e-/X-ray)	338	338

Table 1: Noise and conversion gain parameters measured on detectors A and B.

The readout noise is extracted from a set of 50 dark images. After averaging and subtracting this average dark image from all of the other dark images, the histogram is taken of which the standard deviation σ is the readout noise of the detector. The best published amorphous-silicon based TFT detectors using active pixels show readout noise levels between 900 and 2500 electrons [1,2]. The readout noise in a CMOS detector using a 3T pixel concept is largely determined by the √(ktC)-noise generated by the pixel reset, as the circuit noise is very low. For low dose applications (HS mode), the total capacitance of the pinned photodiode (C1, Figure 2) is designed as small as possible, tuned to the electron charge corresponding to the required saturation dose.
The conversion gain (e^-/X-ray photon) is calculated straightforwardly from the net signal for a certain entrance dose for a given pixel size. These values are used to calculate the *Ne* (equation (1)), which in turn is the most important factor in evaluating DQE at low dose and NED.

3.2 DQE calculation at very low dose for detector A and B

The DQE(f) curves are extracted from images according to the IEC 62220-1 standard. For high-dose conditions, the calculated DQE(f) for both sensitivity modes settings (HS and HDR) are shown in Figure 3.

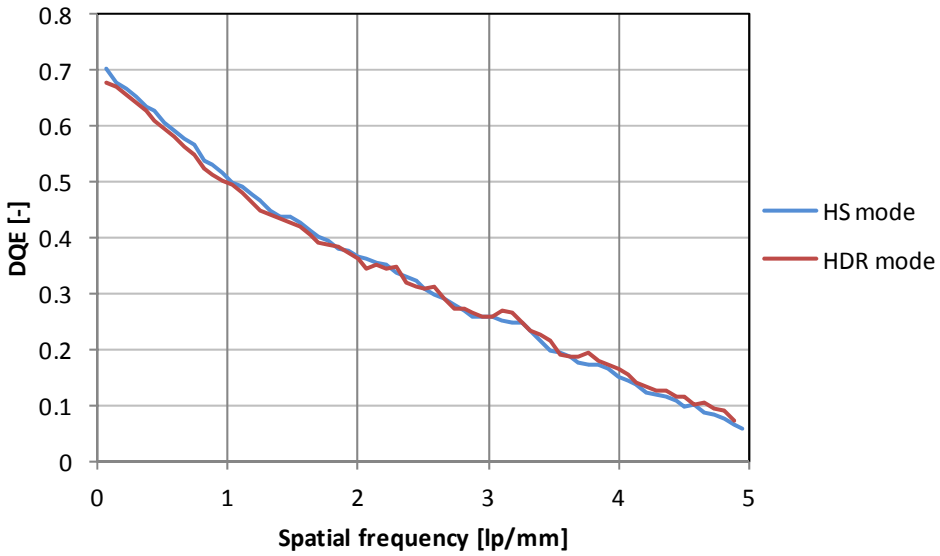

Figure 3: High dose DQE(f) performance in HS and HDR pixel sensitivity modes

To investigate the performance of the detector at very low dose levels, the selected region-of-interest (ROI) of the detector was restricted to 300 lines, to increase the frame-rate to 160fps. At these frame rates, the dose per frame could be reduced to nearly 2nGy, to allow the investigation of DQE(f) at very low dose levels. The measurement results, together with the model calculations, are shown in Figure 4 for detector A and in Figure 5 for detector B.

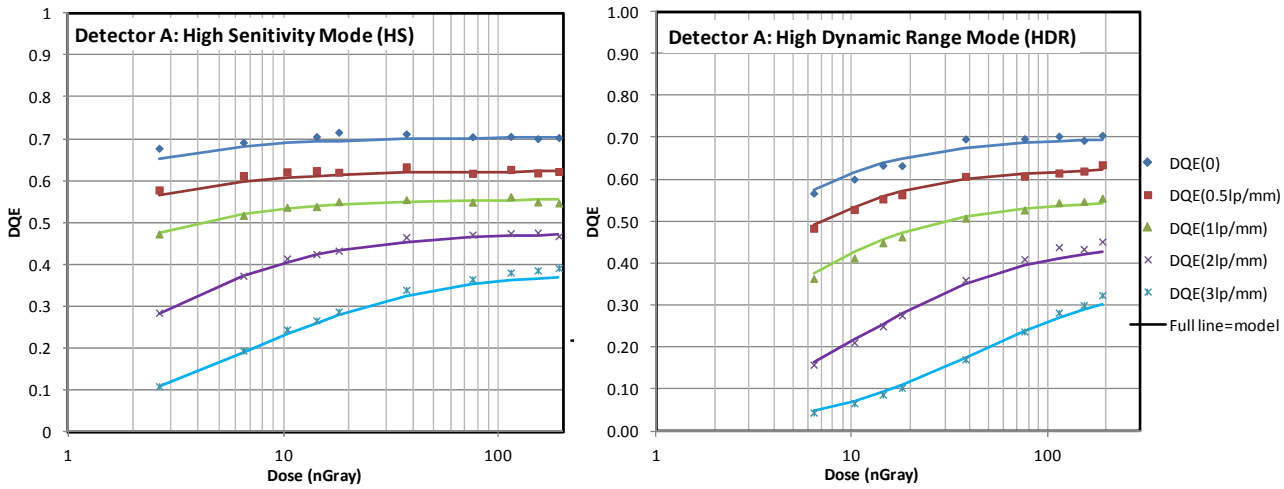

Figure 4: Detector A, DQE versus dose at different spatial frequencies for both pixel sensitivity settings

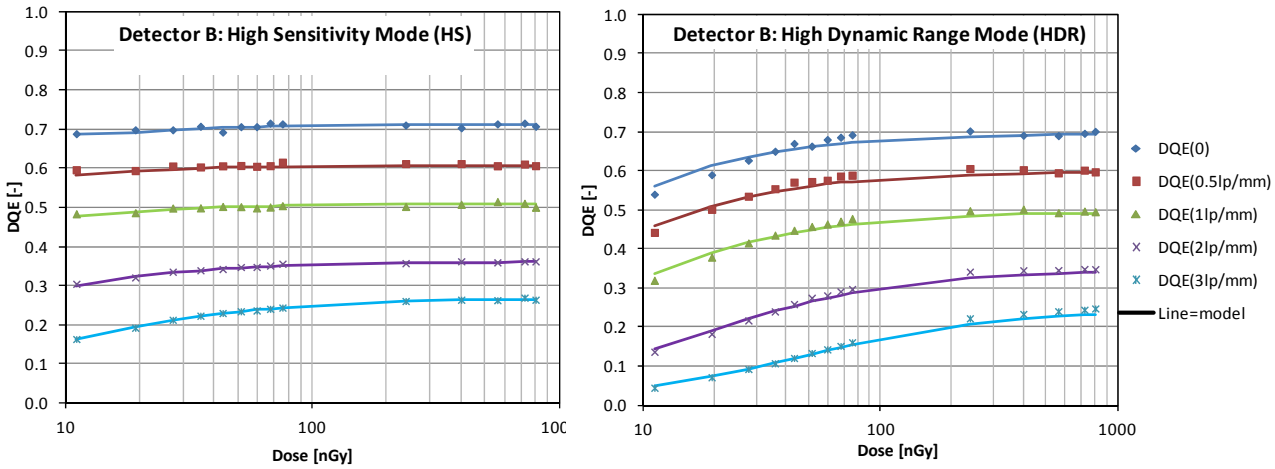

Figure 5: Detector B, DQE versus dose at different spatial frequencies for both pixel sensitivity settings

The degradation of DQE versus dose is less for detector B compared to detector A because of the higher conversion gain of the optical stack, as expected by the equations. For both detectors, the decrease in DQE starts at higher dose levels for HDR mode compared to HS mode because of the higher readout noise level.

The above results show that we can reliably predict the DQE(f) performance at low dose from the high dose DQE(f) measurements.

3.3 NED performance for detector A and B

The NED is defined as the X-ray dose for which the signal noise equals the readout noise of the detector. The readout noise can be extracted from measured dark images as described in section 3.1. Performing the same operation on "white" images (images with uniform illumination) captured at different dose settings, results in a curve representing the total noise in the image at the different dose settings. The total noise includes the X-ray shot noise as well as the detector readout noise. The intersection of this curve with the NED level (equals $\sqrt{2}*\sigma_{read\_noise}$) indicates the NED dose level. The measurements performed on both detectors in both HS and HDR mode are shown in Figure 6 for detector A and in Figure 7 for detector B.

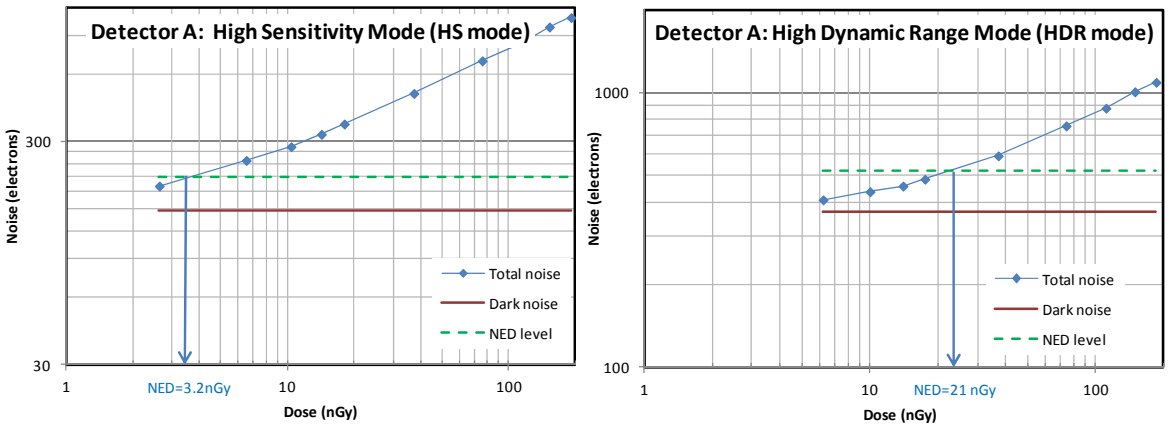

Figure 6: Noise Equivalent Dose (NED) measurements for HS and HDR modes for detector A

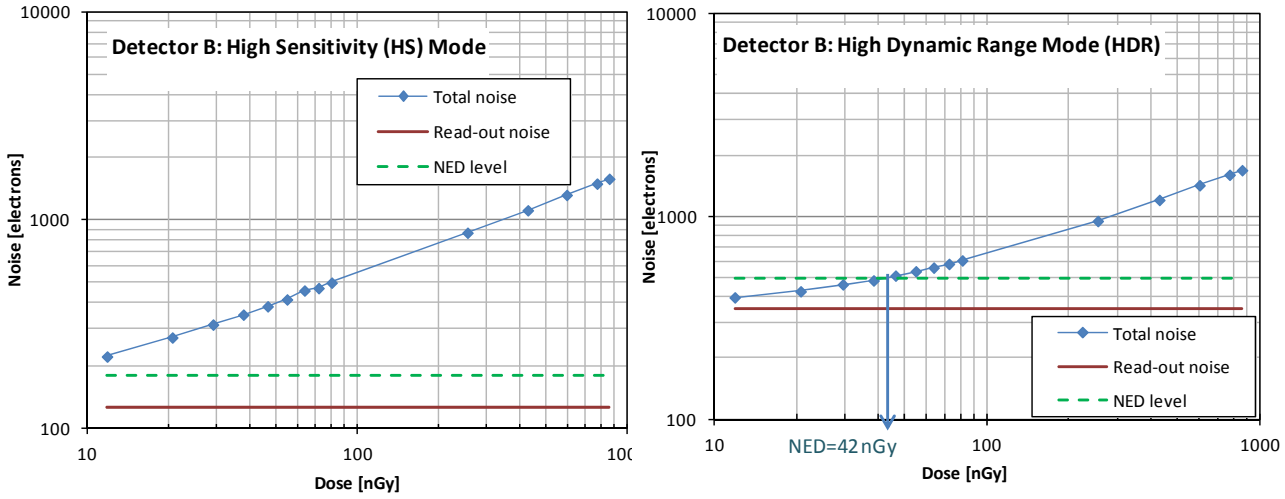

Figure 7: Noise Equivalent Dose (NED) measurement for HS and HDR modes for detector B

The results show that the HS mode has a substantial lower (better) NED compared to the HDR mode because of the lower readout noise, and that detector B has a lower NED than detector A because of the higher conversion factor and better MTF. The NED value of the HS mode of detector B is lower than the lowest measured dose level. At this point, the analytical model as derived in equation 3 can be useful. The result of applying this equation for the 4 different situations are shown in Table 2

NED calculation	*Detector A*		*Detector B*	
	HS	*HDR*	*HS*	*HDR*
Pixel size (μm^2)	99	99	99	99
Readout noise (e^-)	140	340	130	340
Conversion factor (e^-/X-ray)	490	490	338	338
$<MTF^2(f)/DQE(f)_{high\_dose}>$	7.15	7.15	6.20	6.20
Photon fluence	30174	30174	30174	30174
NED (nGy) Calculated	3.9	23.3	6.2	42.4
NED (nGy) Measured	3.2	21.0	<12	42.0

Table 2 Calculated NED values for both HS and HDR modes, for both detectors A and B

It can be concluded that the simulated and measured NED values compare fairly well.

4. ANALYSIS FOR DETECTOR C AND D

4.1 Description of both detectors C and D

In this section, two further detectors are investigated on NED performance. They contain pixels with a pitch of 135um. Detector C has a CsI-coated FOP in its optical stack. Detector D has the same sensor but the FOP has been omitted and the CsI scintillator is directly attached to the sensor. The different parameters for both detectors have been measured as defined in section 3.1, the results are shown in Table 3.

Detector		*HS*	*HDR*
C	Readout noise (e-)	76	160
	Conversion gain (e-/photon)	330	330
D	Readout noise (e-)	76	160
	Conversion gain (e-/photon)	970	970

Table 3 Noise and conversion gain parameters measured on detectors C and D.

The conversion gain has more than doubled by omitting the FOP from the optical stack of the detector. The influence of this gain on DQE and NED will be investigated.

4.2 DQE calculation for very low dose for detector C and D

The same procedure as described in section 3.2 has been applied. The results for both detectors in both sensitivity modes are shown in Figure 8 for detector C and in Figure 9 for detector D.

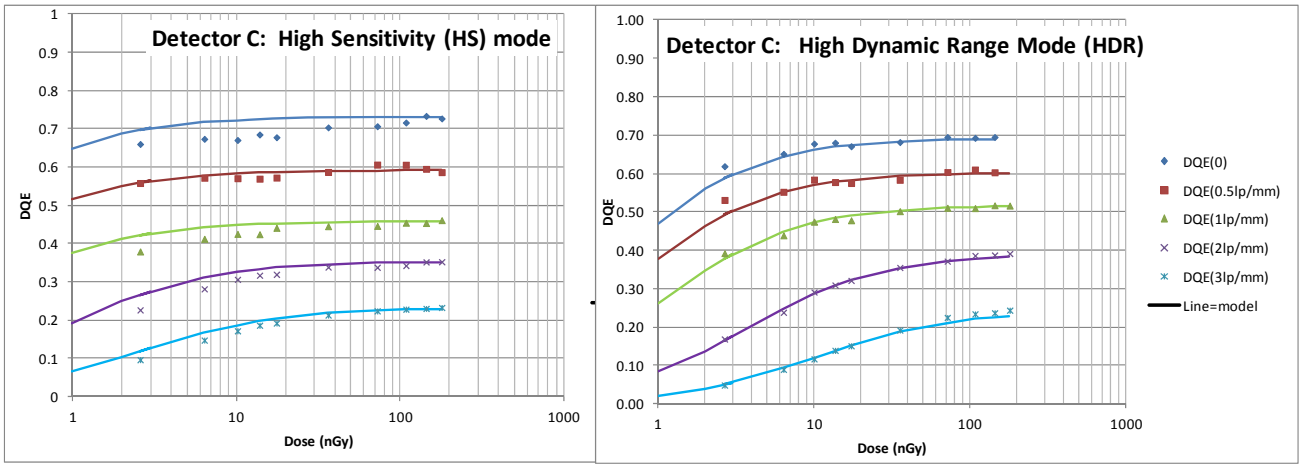

Figure 8: Detector C, DQE versus dose at different spacial frequencies for both sensitivity settings

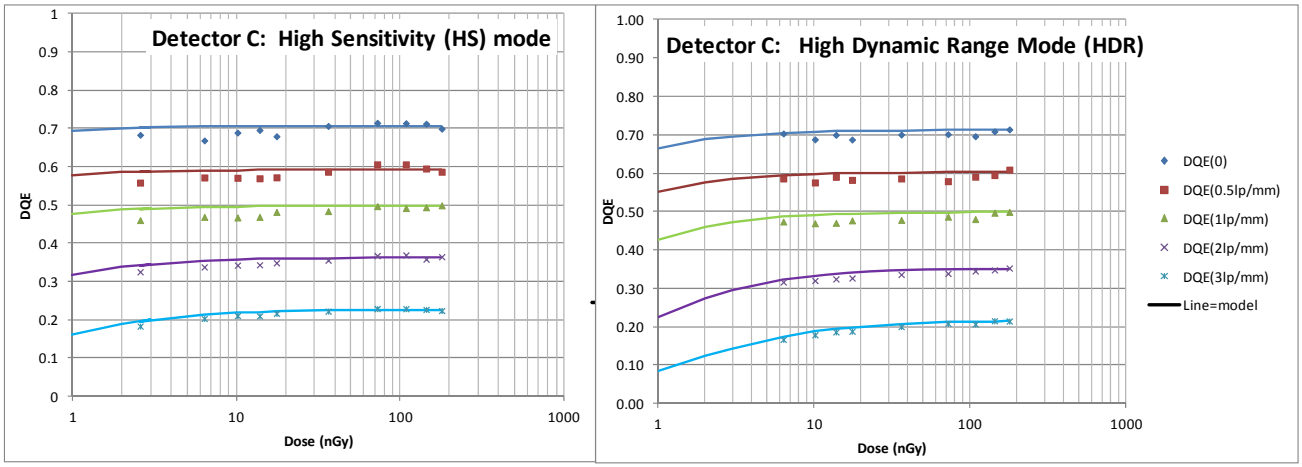

Figure 9: Detector D, DQE versus dose at different spacial frequencies for both sensitivity settings

The figures indicate that omitting the FOP increases the low-dose performance considerably, because of the higher light output of the optical stack. A consequence of this higher light output is that detector D has a lower saturation dose level than detector C. Leaving the FOP out increases the risk on X-ray induced silicon damage resulting in sensor performance degradation, most importantly due to an increase of the pixel leakage current but also degradation of the readout circuitry. In the detectors discussed in this paper, this has been mitigated as part of the sensor design. Another point of attention is the impact on image quality of direct X-ray absorption events in the silicon structure, especially for low X-ray beam energy conditions.

4.3 NED calculations for detector C and detector D

The photon fluence was calculated for the X-ray source at 50kV with an added 22mm Al filtration. This X-ray source setting was needed to achieve a very low dose level on the detector, required to validate the NED model for different fluence settings. Because of the very low NED values, direct measurements of these values are very difficult as explained above. Only the NED value for detector C in HDR mode could be extracted from the measurement to be 3.8nGy, corresponding very well with the calculated value. All calculated values for both detectors are shown in Table 4 .

NED calculation	Detector C		Detector D	
	HS	HDR	HS	HDR
Pixel size (μm^2)	135	135	135	135
Read-out noise (e^-)	76	160	76	146
Conversion factor (e^-/X-ray)	375	375	970	970
$<MTF^2(f)/DQE(f)_{high\_dose}>$	4.70	4.70	4.50	4.50
Photon fluence	23233	23233	23233	23233
NED (nGy)	0.9	4.0	0.1	0.5

Table 4: Calculated NED values for both HS and HDR mode and for both detectors C and D

The impact of the higher conversion factor on the NED value after omitting the FOP is significant, especially in HS mode. The DQE graphs of both detectors in the shot noise limited regime are almost equal as shown in Figure 10. This implies that the NED values of detector C and D (in HR and HDR mode) are directly comparable and indicate the impact of the different conversion factor of both detectors.

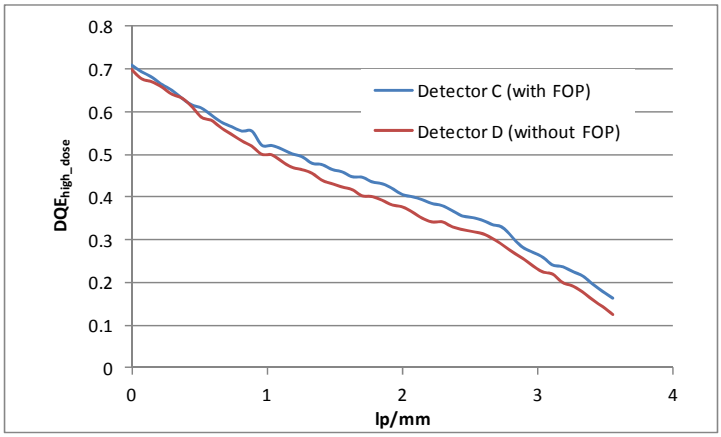

Figure 10 DQE_{high_dose} comparison for both detectors C and D

Since omitting the FOP results in a lower saturation dose level, it is modeled what the difference is when detector C and detector D would have the same saturation dose level. A higher saturation dose level of detector D requires a higher charge capacity for the pixel. The impact of this higher capacity on the low dose performance of the detector is illustrated in Figure 11 below. The *R(0, dose)*, see equation 5, is plotted for detector C and D in HS mode as summarized in table 4 and for detector D assuming a similar saturation dose level as detector C. It can be observed that a higher conversion factor will lead to a better performance in low dose at similar saturation dose levels, when operating the detector in HS mode.

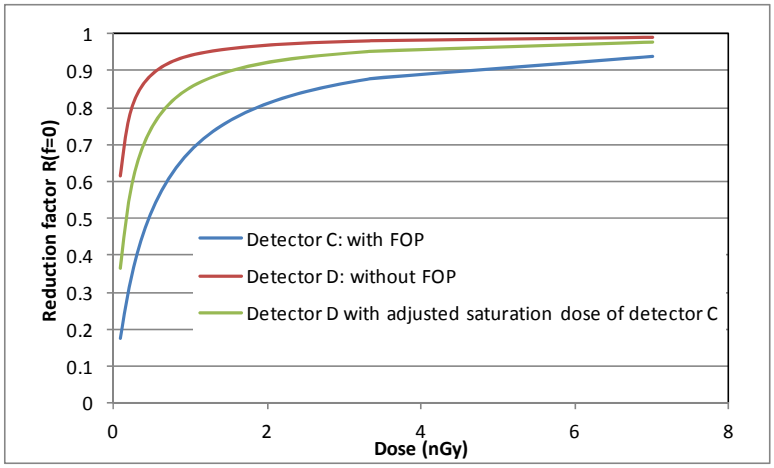

Figure 11 R(0, dose) for three different situations: detector with low conversion factor (C), detector with high conversion factor (D) and detector with a high conversion factor and same saturation dose as detector (C) with low conversion factor (D, adjusted).

5. CONCLUSIONS

In this paper, an analytical model for describing the DQE(f) degradation at very low X-ray dose conditions is presented and validated. The input parameters for this model are extracted from images captured in the higher, shot-noise limited dose regime.

Also an analytical model is derived for calculating the noise equivalent dose (NED) for the High Sensitivity and High Dynamic Range settings of the different detectors. This model enables to calculate the NED value from parameters obtained from higher dose measurements.

Applying both models (DQE and NED) to four different detectors configurations, both operating in HS and HDR mode, showed excellent agreement with measurements under all tested conditions.

These models allow the optimization of X-ray detectors design parameters, like the sensor charge capacity in combination with the conversion gain of the optical stack [3]. An optical stack with a high conversion gain is mostly advantageous for low dose image quality. The required increase in charge capacity to maintain saturation dose will increase the readout noise of the detector, but the relative increase will be less compared to the increase in conversion gain of the stack. It will result in better NED and DQE(f) performance at very low dose.

It is shown that omitting the FOP from the optical stack greatly improves the low dose performance of the detector. Drawbacks are the potential increase of total ionization dose related performance degradation, e.g. the increase in dark current of the sensor, and the impact of the increase of direct X-ray absorption events on the image quality.

6. ACKNOWLEDGMENT

We are grateful to all members of the CMOS design group and the optical stack design and assembly group of Teledyne DALSA. Additionally, we would like to thank Albert Huizinga and Willem Hoekstra for their help on capturing the huge amount of image data. Thanks also to Alexander Zyazin for the valuable scientific discussions.

7. REFERENCES

[1] Wu Dali, Safaviana Nader , Yazdandoosta Mohammad Y. , Izadia Mohammed Hadi and Karim S. Karim, "*Electronic Noise Comparison of Amorphous Silicon Current Mode and Voltage Mode Active Pixel Sensors for Large area Digital X-ray Imaging,*" Proc. of SPIE Vol. 7622, (2010)

[2] Larry E. Antonuk, Qihua Zhao, Youcef El-Mohri, Hong Du, Yi Wang, Robert A. Street, Jackson Ho, Richard Weisfield and William Yao, "*An investigation of signal performance enhancements achieved through innovative pixel design across several generations of indirect detection, active matrix, flat-panel arrays,*" Medical Physics, 36 (7), July (2009)

[3] Zyazin A.S.and Peters I.M., "*Complete Optical Stack Modeling for CMOS-based Medical X-Ray Detectors,*" submitted to SPIE Medical Imaging (2015)

[4] Granfors Paul R., Aufrichtig Richard , Possin George E., Giambatista Brian W., Huang Zhong S., Liu Jianqiang and Ma Bing , "*Performance of a 41x41 cm^2 amorphous silicon flat panel x-ray detector designed for angiographic and R&F imaging applications,*" Medical Physics, 30 (10), October (2003).